

In Vivo Plant Flow Cytometry: A First Proof-of-Concept

Dmitry A. Nedosekin,¹ Mariya V. Khodakovskaya,^{2,3} Alexandru S. Biris,^{2,4} Daoyuan Wang,^{2,4} Yang Xu,^{2,4} Hector Villagarcia,² Ekaterina I. Galanzha,¹ Vladimir P. Zharov^{1*}

¹Phillips Classic Laser and Nanomedicine Laboratories, Winthrop P. Rockefeller Cancer Institute, University of Arkansas for Medical Sciences, Little Rock, Arkansas 72205

²Department of Applied Science, Systems Engineering Department, UALR Nanotechnology Center, University of Arkansas at Little Rock, Arkansas 72204

³Institute of Biology and Soil Science, Far-Eastern Branch of Russian Academy of Sciences, Vladivostok 690022, Russia

⁴Nanotechnology Center, University of Arkansas at Little Rock, Arkansas 72204

Received 17 February 2011; Revision Received 22 July 2011; Accepted 26 July 2011

Grant sponsor: National Institute of Health; Grant numbers: R01CA131164, R01EB009230, R01EB000873 and R21CA139373 (to V.P.Z.); Grant sponsor: National Science Foundation; Grant number: DBI-0852737 (to V.P.Z.); Grant sponsor: Department of Defense; Grant numbers: W88XWH-10-2-0130, W81XWH-10-BCRP-CA, and W81XWH-11-1-0129; Grant sponsor: ASTA; Grant number: 08-CAT-03 (to A.S.B.); Grant sponsor: Arkansas Space Consortium; Grant number: UALR19845 (to M.V.K.)

*Correspondence to: Vladimir P. Zharov, Phillips Classic Laser and Nanomedicine Laboratories, Winthrop P. Rockefeller Cancer Institute, University of Arkansas for Medical Sciences, Little Rock, AR 72205, USA

Email: zharovvladimirp@uams.edu

Published online 8 September 2011 in Wiley Online Library (wileyonlinelibrary.com)

DOI: 10.1002/cyto.a.21128

© 2011 International Society for Advancement of Cytometry

• Abstract

In vivo flow cytometry has facilitated advances in the ultrasensitive detection of tumor cells, bacteria, nanoparticles, dyes, and other normal and abnormal objects directly in blood and lymph circulatory systems. Here, we propose in vivo plant flow cytometry for the real-time noninvasive study of nanomaterial transport in xylem and phloem plant vascular systems. As a proof of this concept, we demonstrate in vivo real-time photoacoustic monitoring of quantum dot-carbon nanotube conjugates uptake by roots and spreading through stem to leaves in a tomato plant. In addition, in vivo scanning cytometry using multimodal photoacoustic, photothermal, and fluorescent detection schematics provided multiplex detection and identification of nanoparticles accumulated in plant leaves in the presence of intensive absorption, scattering, and autofluorescent backgrounds. The use of a portable fiber-based photoacoustic flow cytometer for studies of plant vasculature was demonstrated. These integrated cytometry modalities using both endogenous and exogenous contrast agents have a potential to open new avenues of in vivo study of the nutrients, products of photosynthesis and metabolism, nanoparticles, infectious agents, and other objects transported through plant vasculature. © 2011 International Society for Advancement of Cytometry

• Key terms

photothermal method; photoacoustics; flow cytometry; scanning cytometry; imaging; plants; tomato; nanotechnology

STUDIES of plant-nanoparticle interaction are extremely important to assess the impact of fast-growing nanotechnology products on the environment and agriculture (1,2). Nanomaterials are able to enter into plant cells through cell membranes (3–5) and into the whole plant through roots and plant vascular system (Fig. 1A) inducing changes in plant physiology and gene expression (1,3–9). The accumulation of nanoparticles in plants, especially, in edible ones (6,8), may result in human exposure to these materials. The growing volume of nanomaterials production increases concern over the safety of these nanomaterials to the environment (10). Various novel applications directly oriented to the use of nanotechnology in plants were proposed: delivery of biological molecules into plant cells (4,11), improving herbicide efficacy (12), and enhancing seed germination and plant growth (6,7). Despite this growing number of applications, a methodology for studying fate of nanoparticles in plants in vivo is still lacking. Existing methods of nanoparticle detection in plants often require sample decomposition (8,9,13), and the use of complex methods like transmission electron microscopy (9,14). Magnetic resonance imaging (15) can be used for magnetic nanoparticles only. Main methods for assessment of nanoparticle penetration kinetics include periodic collection of stem and petiole samples from multiple plants (14,16) and the use of invasive analysis methods. Thus, currently there are no methods available for detection of nanoparticles of various types, their quantification, high-resolution mapping (6), and real-time noninvasive monitoring of live plant tissues (2,15,17).

In biomedical applications various techniques based on optical properties of nanoparticles were developed for noninvasive detection and quantification of nanomaterials in live tissues. For real-time monitoring of nonfluorescent nanoparticles in

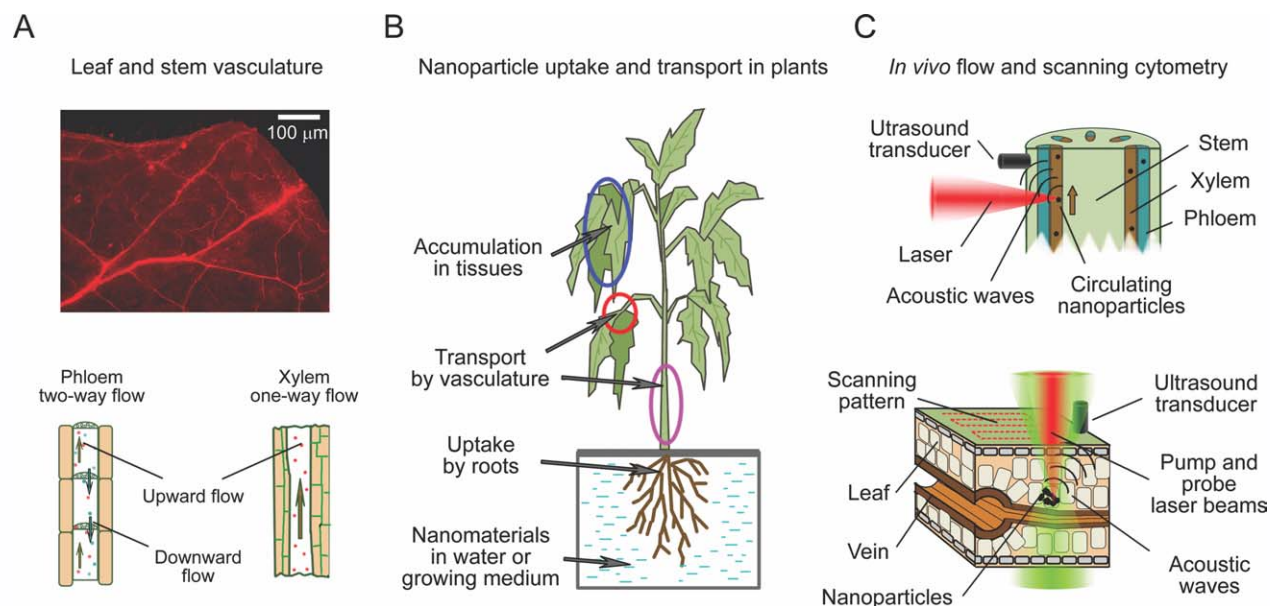


Figure 1. Principles of in vivo plant cytometry. **(A)** Vascular vessels in a tomato leaf (top, autofluorescence, excitation 450 ± 40 nm, emission 600 ± 8 nm) and schematics of flow in main plant vascular tissues (bottom). **(B)** Scheme of uptake, transport, and accumulation of nanomaterials from water or growing medium. **(C)** Principles of in vivo PA plant flow cytometry in a stem (top) and of in vivo PT/PA scanning plant cytometry in a leaf (bottom).

blood and lymph, we proposed in vivo flow cytometry based on the multiplex integration of photothermal (PT) (18–20), photoacoustic (PA) (20–26), Raman (27,28), and scattering (29) techniques. PT and PA flow cytometry (PTFC and PAFC, respectively) methods are based on nonradiative transformation of the absorbed laser energy into heat and acoustic oscillations caused by the fast thermal expansion of the sample. These phenomena are detected either through the changes in optical parameters of the sample or by an ultrasound transducer attached to its surface. We have demonstrated applications of this noninvasive technique for real-time monitoring of blood cells in different functional states (e.g., normal, apoptotic, and necrotic), circulating tumor cells (melanoma, breast, squamous), bacteria (e.g., *Escherichia coli* and *Staphylococcus aureus*), and various nanoparticles and dyes in blood and lymph flow (20–26,30). Scanning PT/PA cytometry was used for the nanoparticle quantification and imaging of tissue samples in vitro and in vivo (23,24,31). Other groups have explored various modifications of the fluorescent methods which have shown promise in the detection of labeled hematopoietic stem cells, GFP-expressing cells, and tumor cells (32–38). Nevertheless, the applications of fluorescence-based technology still needs to overcome such challenges as fluorescent tags' cytotoxicity, undesirable immune response to the tags, and low depth of penetration (below $200 \mu\text{m}$), allowing to assess small ($50\text{--}100 \mu\text{m}$) superficial microvessel only with slow flow (32–38).

Herewith, we introduce in vivo plant flow cytometry for real-time analysis of nanoparticle transport in plants and demonstrate integration of the method with the multispectral scanning cytometry that we have previously developed (6,31).

The main goal of in vivo plant flow cytometry is to provide a real-time detection of objects transported by the plant vascular system (2). A natural long-distance transport in plants occurs in xylem or phloem tissues (Fig. 1A). Water and nutrients consumed by roots from soil are transported by xylem to the leaves, whereas phloem moves photosynthates, amino acids, and electrolytes originating in the leaves to the rest of the plant (17). For large tomato plants, the average linear flow velocity in xylem was reported to be 8 and 2 mm/s during the day and night hours, respectively (17). In phloem the flow is osmotically generated by the gradient in solutes concentration (39), the corresponding flow velocity was reported to be in the range from 0.2 to 0.4 mm/s (17). As it has been demonstrated previously (6–8), nano-sized materials are able to enter plant roots (Fig. 1B). Possible mechanisms include a standard osmotic pressure-driven transport through the pores that are present in cell walls and intercellular plasmadesmata, or via the highly regulated symplastic transfer (9). Thus, plants may uptake nanoparticles, transport them through xylem, and finally accumulate these nanomaterials in various tissues.

To prove the concept of in vivo flow cytometry in plants, we addressed two aspects of plant-nanoparticle interaction: kinetics of nanoparticle uptake and nanoparticle accumulation in tissues. Uptake kinetic was studied in real time by in vivo PA plant flow cytometry, while PT/PA scanning cytometry was used to detect nanoparticles accumulated in various tissues (Fig. 1C). For this study, we selected quantum dot (QD)-carbon nanotube (CNT) conjugates as triple (PT, PA, and fluorescent) contrast agents (40). QDs are typically used as contrast agents for fluorescent imaging (40–43). CNTs have found applications in PT therapy (44), in vivo blood and lymph

PAFC (21,25,27), and PA tomography (45,46). The conjugation of QDs with CNTs combines the high-fluorescence quantum yield associated with QDs (43) and the strong light absorption of CNTs.

METHODS

QD-CNT Conjugates

Synthesis. Single-walled CNTs (hereinafter referred to as CNTs) were synthesized over the Fe-Co/MgO catalyst using the RF-CCVD method and methane as the carbon source (47–49). CNTs were functionalized with NH_2 groups through a three-stage treatment: formation of CNT-COOH groups in $\text{H}_2\text{SO}_4/\text{HNO}_3$ (3:1), followed by SOCl_2 treatment that produced CNT-COCl groups, and final reaction with ethylene diamine that gave CNT- NH_2 product. Water-soluble QDs with a CdSe core and a ZnS shell were synthesized according to established protocol (50) and were functionalized with mercaptopropionic acid (MPA) (51,52). The conjugation of CNT- NH_2 and QDs-MPA was performed in an aqueous solution (53) with the final (weight/weight) ratio of QDs/CNTs set as 1/100. The coupled QD-CNT conjugates (referred as QD-CNTs) were found to be stable: no evidence of QD-CNTs breaking apart was found after intensive sonication.

Instrumentation. The high-resolution transmission electron microscope (HR TEM JEM-2100F, JEOL Inc.) at an acceleration voltage of 200 kV was used for imaging QDs on the surface of CNTs (Fig. 2B). The UV-Vis-NIR optical absorption spectra of the samples (Fig. 2D) were recorded in 1 cm path length quartz cells by using a Shimadzu double-beam spectrophotometer UV-3600 with three detectors. The fluorescent emission of QD-CNTs (Fig. 2D) and the QDs' quantum yield (QY) were determined with the use of Varian Cary Eclipse Fluorescence Spectrophotometer and Rhodamine B/ethanol solution (QY of 0.95 in ethanol) as a comparative standard (54). Samples in 1 cm cuvette were excited at 344 nm, and fluorescent light was collected in the wavelength range of 580 to 620 nm.

Plant Model System

Tomato seeds were surface-sterilized, germinated, and grown on sterile Murashige and Skoog (MS) medium as previously described (6). Thirty-day-old tomato plants (cv. Micro-Tom) with an average stem length of 5 to 10 cm were used in all experiments.

The kinetic of QD-CNT uptake from the water was monitored in vivo in intact tomato plants transferred from agar medium to a tube with a regular water. First group (3 plants) remained in the water throughout the entire experiment (control). A second group (9 plants) was used to monitor the flow of QD-CNTs inside the plants tissues (experimental plants). Control PA signals (in the absence of QD-CNTs) were acquired from control plants and from experimental plants before the introduction of nanoparticles. After the control recordings, 200 μl of 25 $\mu\text{g}/\text{ml}$ QD-CNT solution were added to the water in a tube containing the plant (Fig. 1B) and PA

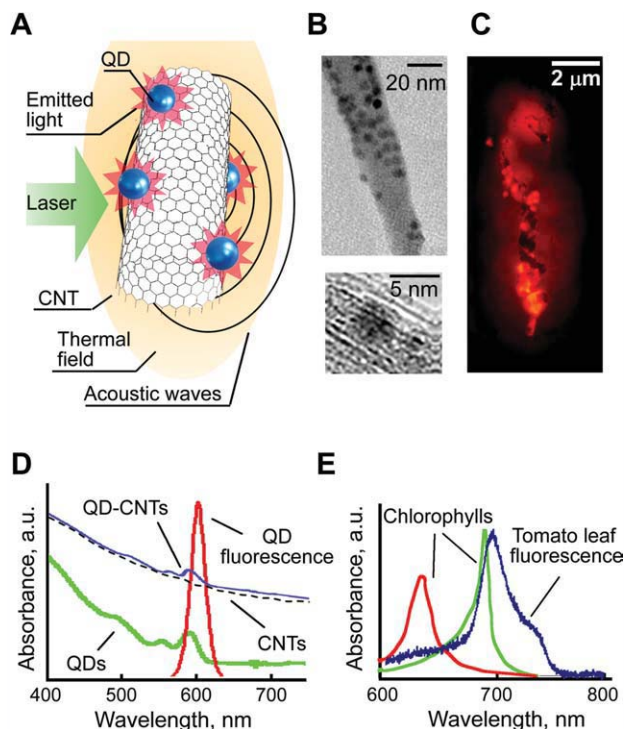


Figure 2. QD-CNTs as multimodal PT, PA, and fluorescence contrast agents. (A) Schematic of laser-induced phenomena in QD-CNTs. (B) TEM image of multiple QDs on a CNT surface. (C) Fluorescent image of a QD-CNT cluster (excitation 450 ± 40 nm, emission 600 ± 8 nm). (D) Absorption spectra of QDs, CNTs, QD-CNTs, and QD emission spectrum. (E) Autofluorescent spectra of a tomato leaf compared to typical absorption spectra of chlorophylls. [Color figure can be viewed in the online issue, which is available at wileyonlinelibrary.com.]

signals were recorded for 1 h from the mid-vein of a leaf or from the main stem. Experiments were repeated for each tomato plant serving as independent biological replicate.

Accumulation of QD-CNTs in tomato plants was studied with a focus on leaf examination in 30-day-old plants grown for 10 days on a MS medium supplemented with QD-CNTs (at a concentration of 50 $\mu\text{g}/\text{ml}$). Leaves of tomato plants grown on a standard MS medium were used as a control (total six leaves from three different plants). For each leaf from one to three areas with a size of $500 \times 500 \mu\text{m}$ were analyzed to estimate background PT/PA signals. A tomato leaf was prepared for microscope calibration by local injection of 30 μl of a 0.5 mg/ml QD-CNT solution into the leaf tissues. For imaging convenience whole tomato leaves were detached from a stem and deposited for observation on a glass slide under a coverslip (Fig. 3C).

Integrated Plant Cytometer

The prototype of a plant cytometer (Fig. 3A) was built on the technical platform of an Olympus invert IX81 microscope (Olympus America, Inc., Center Valley, PA) with incorporated scanning PT/PA setup, PA flow cytometer, and conventional fluorescent wide-field imaging module.

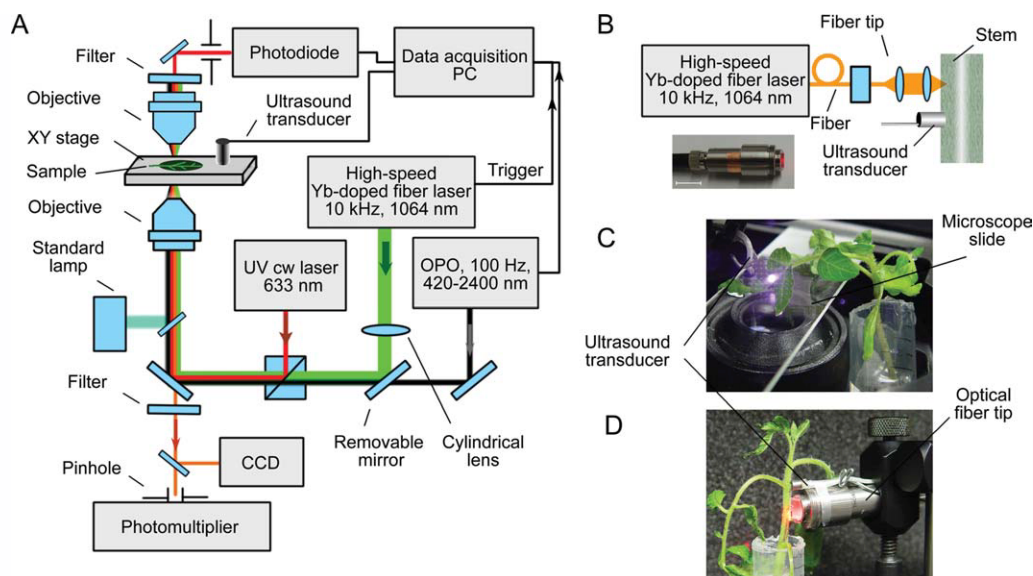


Figure 3. In vivo integrated flow and scanning cytometry with PT, PA, and fluorescent detection schematics. **(A)** Schematic of the integrated setup. **(B)** Customized optical fiber tip for laser radiation delivery to plants. **(C)** Scanning cytometry in a leaf with the microscope schematic. **(D)** Optical fiber-based flow cytometry. [Color figure can be viewed in the online issue, which is available at wileyonlinelibrary.com.]

Scanning PT/PA microscope-cytometer implemented a tunable optical parametric oscillator (OPO, Opolette HR 355 LD, OPOTEK, Carlsbad, CA) with the following parameters: tunable wavelength range, 420 to 2,500 nm; pulse width, 5 ns; pulse repetition rate, 100 Hz; and beam diameter on sample, 1.2 μm . XY translation stage (H117 ProScan II, Prior Scientific, Rockland, MA) was used for raster scanning of the plant sample (Fig. 3C). The PT (also referred to as thermal-lens) effect was manifested by defocusing of a probe He-Ne laser beam (wavelength, 633 nm; power, 1.4 mW; model 117A, Spectra-Physics, Santa Clara, CA) at a photodetector (PDA36A, 40 dB amplification, ThorLabs, Newton, NJ) pinhole plane after the sample. The PT signal had the linear positive asymmetric component associated with fast heating and slower cooling effects and a nonlinear sharp negative peak associated with nano-bubble formation around the overheated zones (Fig. 4C) (22). Laser-induced acoustic waves in the sample were detected by an ultrasound transducer (XMS-310, Panametrics-NDT, Olympus NDT, Center Valley, PA) and amplified (preamplifier model 5662B; bandwidth, 50 kHz–5 MHz; gain 54 dB; Panametrics NDT, Olympus NDT Inc., Center Valley, PA). The transducer was placed directly onto a sample with water layer used to improve acoustic coupling. The PA signal had a classic bipolar shape transformed into a pulse train due to reflections and diffraction effects (Fig. 4D).

In vivo PA plant flow cytometer was equipped with a high pulse rate Yb-doped fiber laser (MOPA-M-10, MultiWave Photonics, Portugal) with the following parameters: wavelength, 1,064 nm; pulse width, 10 ns; pulse repetition rate, 10 kHz to 0.5 MHz; energy fluence range on sample surface, 0.01 to 1.0 J/cm². Laser radiation was delivered either through the microscope based setup described above or through a 400 μm multi-mode fiber (M28L05, Thorlabs, Newton, NJ) having a custom

miniature tip with cylindrical optics (Fig. 3B). Both the transducer and the optical-fiber tip were fixed in a holder and were gently touching the plant stem (Fig. 3D). For both the microscope based setup and for the fiber tip the laser beam spot in the sample had linear shape with the dimensions of 200 \times 150 and 50 \times 400 μm , respectively.

The analysis of PT and PA signals was performed by a PC (Dell Precision 690) equipped with a high-speed (200 MHz) analog-to-digital converter board PCI-5124 (National Instruments, Austin, TX), which was used to acquire signals from the transducer and photodiode. Control of the setup and signal acquisition/processing was realized via custom software module (LabView 8.5 complex, National Instruments, Austin, TX). PT/PA images were constructed by plotting PT/PA signals in a XY coordinate plane with the grey shading. All the PT/PA signals with amplitudes not exceeding 5σ level (five times the standard deviation of the background signal in the absence of the excitation beam) were plotted in a black color.

Fluorescent wide-field imaging of the QDs was performed with the following filter: excitation 450 ± 40 nm, emission 600 ± 8 nm, and a single band dichroic mirror 510 nm (Semrock, Rochester, NY). Exposure time of fluorescent imaging was 200 ms for leaves and 5 s for roots. For leaves this exposure time corresponded to a “black” image of a control plant leaf (the maximal image pixel intensity below 5/256 level in a greyscale mode). This exposure duration was selected experimentally as the shortest one from a set of leaf images taken from five different control plants. The fluorescent spectra of the samples were obtained by spectrophotometer (USB4000, Ocean Optics, Dunedin, FL) with a fluorescent filter featuring a long-pass emission filter transmitting light with wavelengths longer than 600 nm (Semrock, Rochester, NY). The optical transmission and fluorescent images of selected

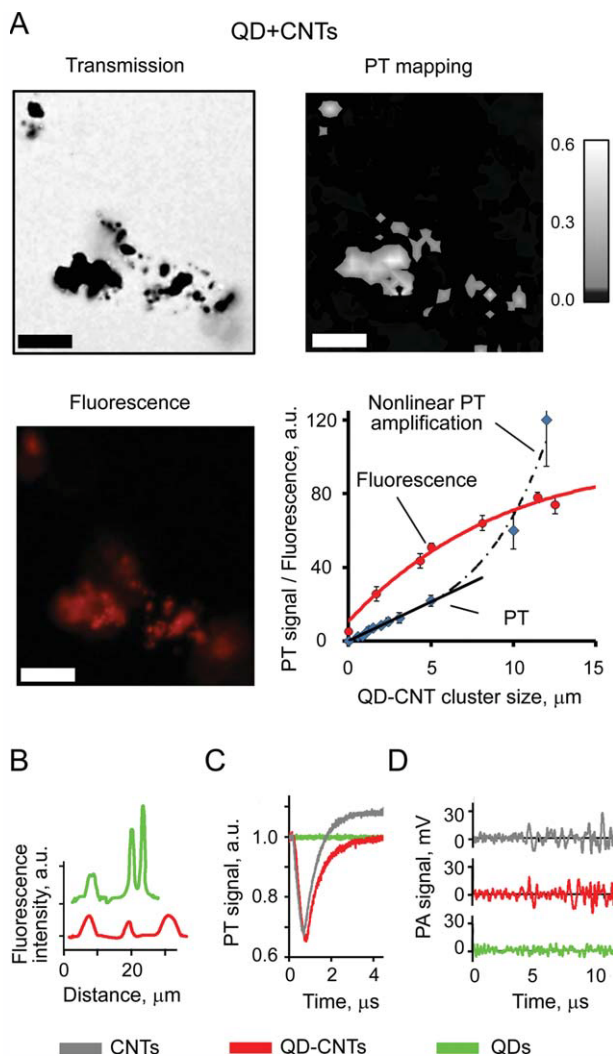


Figure 4. In vitro detection and imaging of individual QDs, CNTs, and QD-CNTs. (A) Transmission, PT, and fluorescent imaging of QD-CNTs. Calibration graph represents PT signals and fluorescence intensity for QD-CNTs aggregates of various sizes. Laser parameters: energy fluence of 0.05 J/cm^2 , wavelength 903 nm , scan step $1 \mu\text{m}$. Scale bar: $5 \mu\text{m}$. (B) Line profile for fluorescent intensity of $5 \mu\text{m}$ QD and QD-CNT clusters. (C) PT and (D) PA signals from QD, CNTs, and QD-CNT clusters. Laser parameters: 903 nm , 0.05 J/cm^2 . [Color figure can be viewed in the online issue, which is available at wileyonlinelibrary.com.]

plant parts were obtained with a color CCD camera (DP-72, Olympus, Center Valley, PA).

Statistical Analysis

Results were expressed as means plus/minus the standard error of at least three independent experiments. Results for independent biological replicates were compared by unpaired *t*-test. $P < 0.05$ was regarded as statistically significant. In PAFC mode the increase in PA signal amplitude exceeding 5σ criterion (five times standard deviation of the baseline) was considered statistically significant, i.e. corresponding to QD-CNTs. MATLAB 7.0.1 (MathWorks) software was used for the statistical calculations.

RESULTS

Characterization of QD-CNTs

The hybrid nanoparticles synthesized by conjugation of QDs and CNTs were selected for verification of the in vivo plant flow and scanning cytometry modalities. The success of conjugation was proved by HR TEM imaging (Fig. 2B) that demonstrated the presence of multiple QDs on the exterior surface of the CNTs. Absorption spectrum of QD-CNTs slightly differed from that of pure CNTs (Fig. 2D), featuring small increase at the wavelengths corresponding to the QDs' absorption maximum. QD-CNTs demonstrated intensive fluorescence (Fig. 2C).

At the first stage of in vitro tests we performed multimodal imaging of QD-CNT conjugates to assess possible changes in imaging contrast due to aggregation (Fig. 2A). QD-CNTs were successfully imaged in vitro by optical transmission fluorescent and PT microscopies (Fig. 4A). Calibration graph based on fluorescent imaging data (Fig. 4A, bottom right) revealed fluorescence quenching (53,55,56) in large QD-CNT aggregates. Comparison of QD-CNT conjugates with aggregates of pure QDs ($2\text{--}5 \mu\text{m}$ sized clusters, Fig. 4B) revealed approximately threefold decrease in fluorescence intensity for the aggregates of the same size. The experiments with Rhodamine B/ethanol solution as a comparative standard also confirmed the decrease in quantum yield from 30% to 7.8% for QDs attached to CNTs.

The calibration graph for PT detection was linear up to $5 \mu\text{m}$ QD-CNT aggregates. With the increase in aggregate size or at higher laser energy, the nonlinear PT signal amplification was observed. The light absorption of individual QDs in near-infrared (NIR) range selected for plants imaging was relatively low. At the wavelength of 590 nm corresponding to QD absorbance maximum signal-to-noise ratio (SNR) was in the range of 4 to 8 for $500 \mu\text{m}$ clusters. Thus, even though QDs have sufficient optical contrast for PT detection (40), QD absorbance in NIR range can be ignored in PT/PA plant studies. A comparison of the amplitudes and, especially, the shapes of PT/PA signals for CNT and QD-CNT clusters (Figs. 4C and 4D) under similar conditions confirmed that the conjugation did not affected PT/PA contrast of QD-CNTs, which was in line with the spectroscopic data (Fig. 2D). As expected, fluorescence of pure CNTs was undetectable under conditions selected.

Thus, the conjugation of QDs and CNTs produced hybrid nanopropes suitable for PA and PT detection as for fluorescent imaging. The PT and PA contrast of the nanoparticles was not changed, however, the fluorescent intensity decreased two to threefold. Fluorescence quenching was observed for large aggregates of QD-CNTs.

In Vivo Plant Flow Cytometry of QD-CNTs in Tomato Vascular System

To study kinetics of nanoparticle uptake by a plant we proposed the use of a PAFC, which provided unique integration of the high sensitivity and noninvasive analysis in thick tissues. In PAFC mode a laser beam was focused into the vessel and interacted with light-absorbing objects transported through plant vasculature (xylem or phloem). The laser wave-

length (1,064 nm) was selected to minimize background signal of the plant tissues. Fast heating of the circulating objects (Fig. 1C, red) by absorbed laser irradiation provided generation of acoustic waves (21) as a result of a fast thermal expansion of the object (PA effects).

First, transport of QD-CNTs through plant vasculature was monitored by PAFC in the leaf mid-vein (Fig. 5A). Close to the petiole, the linear flow velocity was expected to be as high as in the petiole, while leaf structures are thinner than those of a petiole or stem. A microscope was used for precise navigation and focusing of the laser beam onto the vein (Fig. 5A). For the control plants, there were no PA signals with amplitude exceeding 5σ threshold level. PA signals exceeding this level were observed at 5 ± 1.3 min ($n = 5$) after the QD-CNTs were added to the water (Fig. 5B). In all of the experiments, we observed rare PA signals indicating the presence of nanoparticles in plant vasculature (Fig. 5B). The number of PA peaks observed varied for different individual plants (replicates) and was in a range from 2 to 15 peaks per 30 min. Based on our previous experience with PA detection of circulating CNTs in blood and lymph flow (21,22,25) low PA signals could be associated with individual QD-CNTs and large nonlinear PA signals corresponded to 2–5 μm aggregates. Taking into account the average distance between the roots and the detection point (~ 5 cm), as well as the observed appearance delay of 5 min and assuming fast uptake of nanoparticles, the average linear flow velocity in stem can be estimated as 0.2 mm/s, which does not contradict data available in the literature (17).

Secondly, the PA signals were monitored in the plant stem using optical-fiber to deliver laser radiation (Fig. 3B). As xylem bundles are arranged symmetrically around the stem center (Fig. 1C), a fiber tip can easily be positioned against any part of the stem. In the stem, which was thicker than the leaf, laser radiation at 1,064 nm was more strongly absorbed by deep stem structures. Thus, the level of background PA signals was increased three to fivefold: from 2 to 4 mV for a leaf vein to a 10 to 20 mV level for a stem. In addition, the scattering and attenuation of the laser beam in stem tissues led to a decrease in laser fluence, thus, further decreasing sensitivity. Nevertheless, PAFC provided detection of QD-CNTs transported through the stem. As can be seen from the PA trace (Fig. 5C), the first detectable QD-CNTs reached the detection point in as few as 10 min (mean 14 ± 3 min, $n = 4$) compared to an average of 5 min for detection in mid-vein leaves despite shorter travel path from roots to detection zone in a stem.

Thus, PAFC revealed presence of QD-CNTs in plant vasculature. The data obtained in the leaves and in the stems indicate presence both of individual QD-CNT conjugates and of clustered QD-CNTs in xylem flow (Fig. 5). The lower PA background in the leaves provided better conditions for detection of QD-CNTs.

Scanning Cytometry of QD-CNTs Accumulated in Tomato Roots and Leaves

Scanning cytometry was used to analyze spatial distribution of QD-CNTs escaped from vascular system into tomato leaves. Their detection in plant tissues and distribution map-

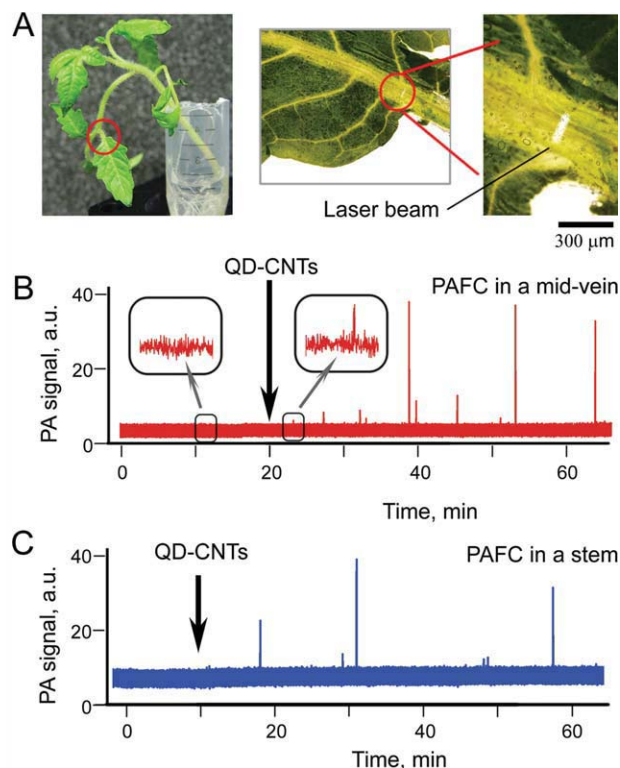


Figure 5. In vivo PA plant flow cytometry of QD-CNTs in tomato vasculature. (A) Linear laser spot in a leaf mid-vein close to petiole. Red lines denote the part of the plant used for monitoring. (B) The trace of PA signals recorded in mid-vein after QD-CNTs were introduced into the water tank. Insets demonstrate enlarged parts of the control trace and the trace with small signal from QD-CNTs. (C) The trace of PA signals from QD-CNTs recorded in the stem (Fig. 3D). Black arrows indicate moment QD-CNTs were introduced into the water tank. The PA traces before introduction of QD-CNTs represent control data. Laser parameters: wavelength, 1,064 nm; pulse width, 10 ns; pulse repetition rate, 10 kHz; laser pulse energy, 20 μJ ; laser spot size in sample: $50 \times 150 \mu\text{m}$ (B) and $100 \times 400 \mu\text{m}$ (C). [Color figure can be viewed in the online issue, which is available at wileyonlinelibrary.com.]

ping were performed by integrated wide-field fluorescent, PT, and PA techniques (Fig. 1C, bottom) to: 1) confirm the presence of QD-CNTs in various plant tissues; 2) analyze the distribution patterns for accumulated nanoparticles; and 3) to demonstrate the improvement in detection accuracy by matching fluorescence of QDs with PT/PA signature of CNTs.

The autofluorescence of leaves (Fig. 1A) and roots affected fluorescent imaging contrast of QD-CNTs. Tomato leaves autofluorescence in the red spectral range was associated mainly with plant chlorophylls (Fig. 2E) and had two maxima near 690 nm and 740 nm (57). The selection of a narrow band filter in the spectral range of maximal QD emission (600 ± 8 nm) increased QDs contrast over plant tissues. Indeed, some bright fluorescent spots were observed apart from the vasculature in plants grown on QD-CNT-containing MS medium (Fig. 6A). QD-CNT clusters with an average size ranging from 5 to 15 μm were distinguished in leaves. The majority of these clusters were observed in leaf tissues close to the vasculature.

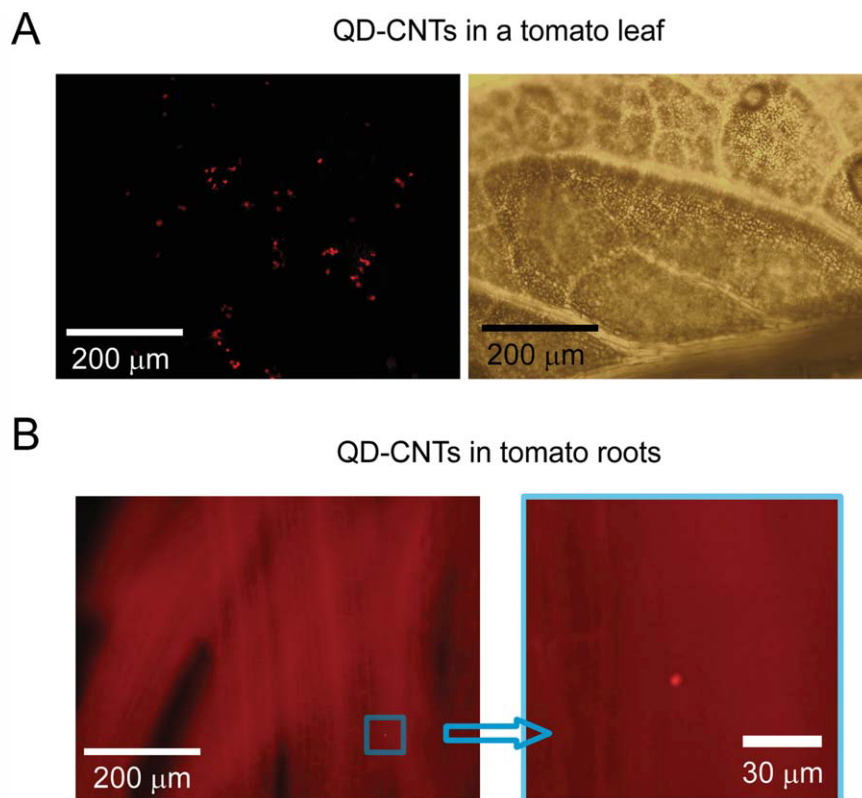


Figure 6. Imaging of QD-CNTs in tomato tissues. **(A)** Fluorescent (left, exposure time, 100 ms) and transmission (right) images of a tomato leaf with accumulated QD-CNTs. **(B)** Fluorescent imaging of tomato roots: image at right magnifies part of the left image (exposure time, 5 s). [Color figure can be viewed in the online issue, which is available at wileyonlinelibrary.com.]

The identification of small QD-CNT clusters in tomato leaves with the fluorescent imaging was difficult due to a very heterogeneous background and the possible attenuation of QD optical emission by plant tissues. In the roots of tomato plants, we were able to identify QD-CNT clusters as small as $2\ \mu\text{m}$ (Fig. 6B). Compared to leaf structures, light-scattering and attenuation in roots were much lower. Thus, fluorescent wide-field imaging of QD-CNTs in plants alone was not sufficient for identification of nanoparticles due to high heterogeneity of plant autofluorescence.

Next, PT/PA scanning cytometry was used to confirm that bright spots discovered in the sample indeed were QD-CNTs. The NIR spectral range of 750 to 950 nm was considered as the most promising for PT/PA plant cytometry as the absorption background from chlorophyll and other plant components in the NIR range was much lower than that in the visible range (Fig. 2E), while the absorption of QD-CNTs decreases only two to threefold in the NIR range compared to that in visible range (Fig. 2D). Moreover, the sensitivity of PT/PA cytometry was enhanced by laser-induced nano- and microbubbles around laser-overheated QD-CNT clusters (25,31) acting as PT/PA signal amplifiers (Figs. 4C and 4D). In particular, the bubbles' expansion and collapse take several microseconds leading to the formation of sharp, negative PT signals as signatures of the strong local absorption associated with QD-CNT clusters (Fig. 4C).

For calibration purposes, a solution containing QD-CNTs was injected into the leaf tissues (Fig. 7A), while another leaf was inoculated with pure CNTs at a similar concentration. These areas were imaged by PT/PA scanning cytometer. The locations of the signals correlated with the incision sites for both CNTs and QD-CNTs. Imaging contrast (as a ratio of signal amplitude from nanoparticles to tissue background) for QD-CNT clusters were in the range of 30 to 40 and 5 to 10 for PT and PA detection, respectively, confirming higher sensitivity of PT technique in thin leaves. The PT images (Fig. 7C) were well-correlated with fluorescence images of the QD-CNTs among the leaf structures (Fig. 7B). There were no PT/PA signals exceeding control signal level acquired from the leaf vasculature, which provided a strong background in the fluorescent images (see blue arrows, Figs. 7A–7C).

Two approaches to the use of a PT/PA scanning cytometry for QD-CNT detection in the leaves of a plant grown on nanomaterial-containing medium were tested: 1) imaging of a small area having abovementioned fluorescing signatures, and 2) imaging of a larger sample area (up to $1 \times 1\ \text{mm}$) having no distinctive fluorescent features. In the first case, we observed high PT/PA signals (SNR in the range of 20–30 similar to those observed for the sample with injected nanoparticles) collocated with the local areas of high fluorescence in the sample (Figs. 7D and 7E). High PT/PA signals were observed

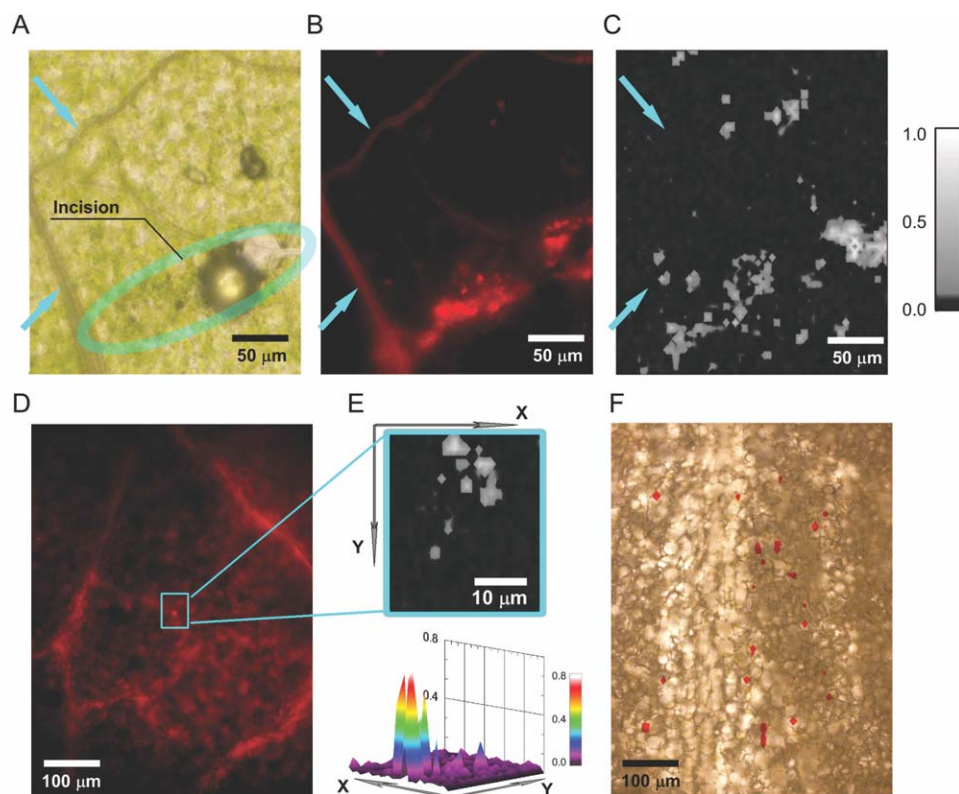


Figure 7. Integrated scanning cytometry of QD-CNTs in tomato leaf using PT, PA, and fluorescent detection methods. (A–C) Transmission, fluorescence, and PT images (903 nm, 1.0 J/cm²) of tomato leaf with the artificially introduced QD-CNTs. Blue arrows indicate leaf vasculature. Fluorescent imaging exposure 200 ms. (D) Fluorescent and (E) PT images of a leaf from 10-day-old tomato plant grown on a QD-CNT containing medium; exposure time, 200 ms. PT image (E) represents two-dimensional map (top) and 3D map of the same area (bottom). (F) Transmission image of a sample having no distinctive fluorescence features overlaid with PT image (red) indicating locations of QD-CNTs.

for 13 sites out of 17 scanned indicating that four sites were identified as containing QD-CNTs incorrectly. Both the amplitudes and the shapes of the PT signals revealed specific features (Fig. 4C) associated with nano- and micro-bubbles' formation around aggregated QD-CNTs. PT imaging of the leaves with no substantial fluorescent signatures (exceeding the level of heterogeneity observed for control plants) revealed presence of multiple PT/PA signals (Fig. 7F) featuring shapes and amplitudes specific to nanomaterials. SNR for observed PT signals was in the range of 5 to 10, suggesting that much smaller aggregates were detected than in the case of the sample with injected nanoparticles. The weak fluorescence for these aggregates could be related either with smaller size or with particles deposition in deeper plant tissues, i.e. with scattering and quenching of fluorescence photons. PT imaging revealed very high heterogeneity of nanomaterial distribution in the sample with the highest density of detected nanomaterials along the main vascular veins (Fig. 7F) and much fewer particles found in areas with only small capillaries. For a typical leaf area of $500 \times 500 \mu\text{m}$ there were 27 ± 12 (7 samples) and 4 ± 3 (4 samples); PT/PA signals were detected near a large vein and near edge of the leaf, respectively.

Thus, PT/PA cytometry confirmed the presence of accumulated nanoparticles and demonstrated higher sensitivity in

detection of smaller aggregates in plant tissues compared to fluorescence imaging.

DISCUSSION

In this article we have presented an integrated fluorescence/PT/PA cytometry with a focus on study nanoparticle uptake kinetics and detection of nanomaterials accumulated in plants. To the best of our knowledge, this is the first demonstration of in vivo noninvasive detection of the nanomaterials accumulated in plant tissues or transported by plant vasculature. PA/PT based cytometry can be applied to a wide range of nanomaterials, with high sensitivity sufficient for detection of even individual nanoparticles and in vascular flow. The experiments in tomato plants demonstrated feasibility of in vivo PA/PT based cytometry with a potential to detect nanomaterials, viruses, bacteria, and other plant disease-associated pathogens or tumor cells (62) in both phloem and xylem tissues, and in vascular system. In Table 1 we summarized potential applications of PT/PA based methods.

PAFC proved to be a robust platform for routine testing ecotoxicological risks of nanomaterials through a rapid and accurate assessment of uptake kinetics. The method is express, simple, and shows potential application with virtually any plants and for a wide range of nonfluorescent nanomaterials.

Table 1. Potential applications for PT/PA scanning and flow cytometry in plants. Comparison with existing methods

APPLICATION	METHOD	SIMPLICITY			LIMITATIONS	REFERENCES
		IN VIVO ANALYSIS	PREPARATION	LOCALIZATION		
Detection of nanomaterials accumulated in plants	Volume analysis after acid digestion	-	-	-	Sample destruction	8,9, and 16
	Optical transmission microscopy	-	+	+	Low depth	9 and 16
	Electron microscopy	-	-	+	Complex sample preparation	9 and 14–16
	MRI	+	+	+	Only magnetic materials	15
Monitoring of nanomaterials uptake	Raman and FTIR spectroscopy	+	+	-	Low sensitivity, large sample volumes	9
	PA/PT scanning microscopy	+	+	+	Absorbance background and light scattering in thick tissues	
	Sampling different plants at selected time intervals, ex vivo analysis (see methods above)	-	-	+	Multiple biological replicates. Low time resolution. Invasive sampling	9
Viruses and pathogens, plant tumor (62)	PA flow cytometry	+	+	+	Absorbance background and light scattering in thick tissues	
	Immunofluorescence microscopy	+	+	+	Autofluorescent artifacts	58
	ELISA of xylem sap, ex vivo	-	-	-	Invasive sap extraction	59
Xylem/phloem transport studies	PT detection and eradication with molecular labeling	+	+	+	Requires labeling of viruses and pathogens	21 and 23
	MRI	+	+	+	Low spatial resolution	17
PA flow cytometry of the contrast agents	Pressure probes	+	-	-	Invasive procedure	60
	Radioisotope labeling	+	+	-	Radioactive probes	61
	PA flow cytometry of the contrast agents	+	+	+		

The study of viruses, bacteria, and other pathogens transported through vascularity of plants may use the principles of *in vivo* PAFC in mammals (21): labeling of objects of interest with functionalized nanoparticles (24) followed by PAFC detection of these labels in the plant. The analysis of transportation dynamics revealed feasibility of another PAFC application for vascular flow velocity studies as on a large scale (presented here roots-leaves transportation by xylem), so as ultralocal flow rate measurement by PA time-of-flight technique (23,25). Noninvasive PAFC should not change sap flow in vasculature. The analysis can be performed even in very thin veins or capillaries of a plant. The applications listed here are feasible not only on a lab bench, but also could be transferred into an agriculture field with the use of a portable fiber laser cytometer presented. Applications of PAFC could include rapid screening of live plants for presence of nanomaterials in vasculature in the case of anthropogenic contamination. One of the main advantages of *in vivo* plant flow cytometry is noninvasive detection and deep tissue assessing. This eliminates limitations on a plant size and makes it possible to avoid flow disturbances usually associated with invasive xylem liquid collection methods. For the large plants and thick tissues PAFC sensitivity is decreased due to a high level of absorption background. However, this drawback can be minimized either by the use of a focused transducer rejecting out-of-focus acoustic waves (23) or by the local laser bleaching of plant chromophores around the detection zone by the use of high energy laser pulses (6).

Scanning fluorescent/PT/PA cytometry provides an opportunity to reveal the fate of nanomaterials penetrated into a plant. First, for nanomaterials having a high fluorescent quantum yield the fluorescent imaging is an obvious choice. However, intensive and heterogeneous autofluorescence of plant tissues decreases imaging contrast and identification accuracy. Such fluorescent techniques like spectral deconvolution, multispectral imaging, and confocal imaging could be used to separate fluorescence of nanomaterials from autofluorescence of plant tissues and, thus, enhance imaging contrast. Still, fluorescent imaging in plants has the same drawbacks as in mammal tissues: the need to consider autofluorescent background and low depth of penetration of fluorescent photons. Second, various nanomaterials like gold nanospheres, gold nanorods, carbon nanotubes, etc. have very high light absorbance. Integration of two modalities in a single scheme provides a highly sensitive detection in optically thin samples ($\leq 100 \mu\text{m}$) by the means of PT detection scheme and analysis in deep tissues with a PA mode. Indeed, the PA technique which is insensitive to scattering background has already demonstrated the possibility of deep tissue imaging in animals (depth penetration of 3–5 cm) (40,43,46) and, as we show here, translation of this schematic to plants is feasible. Nonlinear thermal effects occurring upon absorption of the high energy laser pulses by nanomaterials provide a unique approach to identification of nanomaterials in the plant tissues.

In the current experimental setup, scanning of a small area of 100 to 400 μm in size takes approximately 2 to 10 min. The imaging of a larger area (1 \times 1 mm) with high

resolution can take up to 1 h. Future development of PT/PA scanning cytometry we envision as combination of a high pulse repetition rate laser sources [up to 500 kHz (25)] with an optical scanning system (63). Multispectral PT/PA imaging and spectral analysis is also feasible with the use of successive laser pulses of different wavelengths slightly separated in time (23).

ACKNOWLEDGMENTS

The authors acknowledge the help of Dr. Marinelle Ringer (UALR) in editing this manuscript.

LITERATURE CITED

- Joseph T, Morrison M. Nanotechnology in Agriculture and Food. Nanoforum Report, 2006. Available at: <http://www.nanoforum.org>. Accessed August 10, 2011.
- Ma X, Geiser-Lee J, Deng Y, Kolmakov A. Interactions between engineered nanoparticles (ENPs) and plants: phytotoxicity, uptake and accumulation. *Sci Total Environ* 2010;408:3053–3061.
- Etcheberria E, Gonzalez P, Baroja-Fernandez E, Pozueta Romero J. Fluid phase endocytic uptake of artificial nano-spheres and fluorescent quantum dots by sycamore cultured cells. *Plant Signal Behav* 2006;1:196–200.
- Liu QL, Chen B, Wang QL, Shi XL, Xiao ZY, Lin JX, Fang XH. Carbon nanotubes as molecular transporters for walled plant cells. *Nano Lett* 2009;9:1007–1010.
- Stampoulis D, Sinha SK, White JC. Assay-dependent phytotoxicity of nanoparticles to plants. *Environ Sci Technol* 2009;43:9473–9479.
- Khodakovskaya MV, de Silva K, Nedosekin DA, Dervishi E, Biris AS, Shashkov EV, Galanzha EI, Zharov VP. Complex genetic, photothermal, and photoacoustic analysis of nanoparticle-plant interactions. *Proc Natl Acad Sci USA* 2011;108:1028–1033.
- Khodakovskaya M, Dervishi E, Mahmood M, Xu Y, Li ZR, Watanabe F, Biris AS. Carbon nanotubes are able to penetrate plant seed coat and dramatically affect seed germination and plant growth. *ACS Nano* 2009;3:3221–3227.
- Zhu H, Han J, Xiao JQ, Jin Y. Uptake, translocation, and accumulation of manufactured iron oxide nanoparticles by pumpkin plants. *J Environ Monit* 2008;10:713–717.
- Lin SJ, Reppert J, Hu Q, Hudson JS, Reid ML, Ratnikova TA, Rao AM, Luo H, Ke PC. Uptake, translocation, and transmission of carbon nanomaterials in rice plants. *Small* 2009;5:1128–1132.
- Tiede K, Hassellöv M, Breitbarth E, Chaudhry Q, Boxall ABA. Considerations for environmental fate and ecotoxicity testing to support environmental risk assessments for engineered nanoparticles. *J Chromatogr A* 2009;1216:503–509.
- Torney F, Trewyn BG, Lin VSY, Wang K. Mesoporous silica nanoparticles deliver DNA and chemicals into plants. *Nat Nanotechnol* 2007;2:295–300.
- Perez-de-Luque A, Rubiales D. Nanotechnology for parasitic plant control. *Pest Manag Sci* 2009;65:540–545.
- Doshi R, Braida W, Christodoulatos C, Wazne M, O'Connor G. Nano-aluminum: transport through sand columns and environmental effects on plants and soil communities. *Environ Res* 2008;106:296–303.
- Corredor E, Testillano P, Coronado M-J, Gonzalez-Melendi P, Fernandez-Pacheco R, Marquina C, Ibarra MR, de la Fuente J, Rubiales D, Perez-de-Luque A, Risueno M. Nanoparticle penetration and transport in living pumpkin plants: *in situ* subcellular identification. *BMC Plant Biology* 2009;9:45.
- Huang X, Stein BD, Cheng H, Malyutin A, Tsvetkova IB, Baxter DV, Remmes NB, Verchot J, Kao C, Bronstein LM, Dragnea B. Magnetic Virus-like nanoparticles in *N. benthamiana* plants: a new paradigm for environmental and agronomic biotechnological research. *ACS Nano* 2011;5:4037–4045.
- González-Melendi P, Fernández-Pacheco R, Coronado MJ, Corredor E, Testillano PS, Risueno MC, Marquina C, Ibarra MR, Rubiales D, Pérez-de-Luque A. Nanoparticles as smart treatment-delivery systems in plants: assessment of different techniques of microscopy for their visualization in plant tissues. *Ann Botany* 2008;101:187–195.
- Windt CW, Vergeldt FJ, De Jager PA, Van As H. MRI of long-distance water transport: a comparison of the phloem and xylem flow characteristics and dynamics in poplar, castor bean, tomato and tobacco. *Plant Cell Environ* 2006;29:1715–1729.
- Zharov V, Galanzha EI, Tuchin V. Photothermal imaging of moving cells in lymph and blood flow *in vivo*. *Proc SPIE* 2004;5320:185–195.
- Zharov VP, Galanzha EI, Tuchin VV. Photothermal image flow cytometry *in vivo*. *Opt Lett* 2005;30:628–630.
- Zharov VP, Galanzha EI, Tuchin VV. *In vivo* photothermal flow cytometry: imaging and detection of individual cells in blood and lymph flow. *J Cell Biochem* 2006;97:916–932.
- Zharov VP, Galanzha EI, Shashkov EV, Kim JW, Khlebtsov NG, Tuchin VV. Photoacoustic flow cytometry: principle and application for real-time detection of circulating single nanoparticles, pathogens, and contrast dyes *in vivo*. *J Biomed Opt* 2007;12:051503.
- Galanzha EI, Shashkov EV, Tuchin VV, Zharov VP. *In vivo* multispectral, multiparameter, photoacoustic lymph flow cytometry with natural cell focusing, label-free detection and multicolor nanoparticle probes. *Cytometry A J Int Soc Anal Chem* 2008;73:884–894.
- Galanzha EI, Shashkov EV, Spring PM, Suen JY, Zharov VP. *In vivo*, noninvasive, label-free detection and eradication of circulating metastatic melanoma cells using two-color photoacoustic flow cytometry with a diode laser. *Cancer Res* 2009;69:7926–7934.

24. Galanzha EI, Shashkov EV, Kelly T, Kim JW, Yang LL, Zharov VP. In vivo magnetic enrichment and multiplex photoacoustic detection of circulating tumour cells. *Nat Nanotechnol* 2009;4:855–860.
25. Nedosekin DA, Sarimollaoglu M, Shashkov EV, Galanzha EI, Zharov VP. Ultra-fast photoacoustic flow cytometry with a 0.5 MHz pulse repetition rate nanosecond laser. *Opt Express* 2010;18:8605–8620.
26. Zharov VP. Ultrasharp nonlinear photothermal and photoacoustic resonances and holes beyond the spectral limit. *Nat Photon* 2011;5:110–116.
27. Biris AS, Galanzha EI, Li ZR, Mahmood M, Xu Y, Zharov VP. In vivo Raman flow cytometry for real-time detection of carbon nanotube kinetics in lymph, blood, and tissues. *J Biomed Opt* 2009;14:021006.
28. Shashkov EV, Galanzha EI, Zharov VP. Photothermal and photoacoustic Raman cytometry in vitro and in vivo. *Opt Express* 2010;18:6929–6944.
29. Tanev S, Sun WB, Pond J, Tuchin VV, Zharov VP. Flow cytometry with gold nanoparticles and their clusters as scattering contrast agents: FDTD simulation of light-cell interaction. *J Biophotonics* 2009;2:505–520.
30. Kim JW, Galanzha EI, Shashkov EV, Moon HM, Zharov VP. Golden carbon nanotubes as multimodal photoacoustic and photothermal high-contrast molecular agents. *Nat Nanotechnol* 2009;4:688–694.
31. Nedosekin DA, Shashkov EV, Galanzha EI, Hennings L, Zharov VP. Photothermal multispectral image cytometry for quantitative histology of nanoparticles and micro-metastasis in intact, stained and selectively burned tissues. *Cytometry A J Int Soc Anal Chem* 2010;77:1049–1058.
32. Novak J, Georgakoudi I, Wei X, Prossin A, Lin CP. In vivo flow cytometer for real-time detection and quantification of circulating cells. *Opt Lett* 2004;29:77–79.
33. Georgakoudi I, Solban N, Novak J, Rice WL, Wei XB, Hasan T, Lin CP. In vivo flow cytometry: a new method for enumerating circulating cancer cells. *Cancer Res* 2004;64:5044–5047.
34. Boutrus S, Greiner C, Hwu D, Chan M, Kuperwasser C, Lin CP, Georgakoudi I. Portable two-color in vivo flow cytometer for real-time detection of fluorescently-labeled circulating cells. *J Biomed Opt* 2007;12:020507.
35. He W, Wang HF, Hartmann LC, Cheng JX, Low PS. In vivo quantitation of rare circulating tumor cells by multiphoton intravital flow cytometry. *Proc Natl Acad Sci USA* 2007;104:11760–11765.
36. Tkaczyk ER, Zhong CF, Ye JY, Myc A, Thomas T, Cao Z, Duran-Struuck R, Luker KE, Luker GD, Norris TB, Baker J. In vivo monitoring of multiple circulating cell populations using two-photon flow cytometry. *Opt Commun* 2008;281:888–894.
37. Zhong CF, Tkaczyk ER, Thomas T, Ye JY, Myc A, Bielinska AU, Cao Z, Majoros I, Kesler B, Baker JR, Norris TB. Quantitative two-photon flow cytometry—in vitro and in vivo. *J Biomed Opt* 2008;13:034008.
38. Chang YC, Ye JY, Thomas TP, Cao ZY, Kotlyar A, Tkaczyk ER, Baker JR, Norris TB. Fiber-optic multiphoton flow cytometry in whole blood and in vivo. *J Biomed Opt* 2010;15:047004.
39. Van Bel AJE. The phloem, a miracle of ingenuity. *Plant Cell Environ* 2003;26:125–149.
40. Shashkov EV, Everts M, Galanzha EI, Zharov VP. Quantum dots as multimodal photoacoustic and photothermal contrast agents. *Nano Lett* 2008;8:3953–3958.
41. Kang HG, Tokumasu F, Clarke M, Zhou ZP, Tang JY, Nguyen T, Hwang J. Probing dynamic fluorescence properties of single and clustered quantum dots toward quantitative biomedical imaging of cells. *Wiley Interdiscip Rev Nanomed Nanobiotechnol* 2010;2:48–58.
42. Yong KT, Qian J, Roy I, Lee HH, Bergey EJ, Trampusch KM, He SL, Swihart MT, Maitra A, Prasad PN. Quantum rod bioconjugates as targeted probes for confocal and two-photon fluorescence imaging of cancer cells. *Nano Lett* 2007;7:761–765.
43. Guo Y, Shi DL, Cho HS, Dong ZY, Kulkarni A, Pauletti GM, Wang W, Lian J, Liu W, Ren L, Zhang QQ, Liu GK, Huth C, Wang LM, Ewing RC. In vivo imaging and drug storage by quantum-dot-conjugated carbon nanotubes. *Adv Funct Mater* 2008;18: 2489–2497.
44. Kim JW, Shashkov EV, Galanzha EI, Kotagiri N, Zharov VP. Photothermal antimicrobial nanotherapy and nanodiagnostics with self-assembling carbon nanotube clusters. *Laser Surg Med* 2007;39:622–634.
45. Kim C, Song KH, Gao F, Wang LV. Sentinel lymph nodes and lymphatic vessels: non-invasive dual-modality in vivo mapping by using indocyanine green in rats—volumetric spectroscopic photoacoustic imaging and planar fluorescence imaging. *Radiology* 2010;255:442–450.
46. Pramanik M, Swierczewska M, Green D, Sitharaman B, Wang LV. Single-walled carbon nanotubes as a multimodal-thermoacoustic and photoacoustic-contrast agent. *J Biomed Opt* 2009;14:034018.
47. Dervishi E, Li ZR, Watanabe F, Xu Y, Saini V, Biris AR, Biris AS. Thermally controlled synthesis of single-wall carbon nanotubes with selective diameters. *J Mater Chem* 2009;19:3004–3012.
48. Biris AS, Schmitt TC, Little RB, Li Z, Xu Y, Biris AR, Lupu D, Dervishi E, Trigwell S, Miller DW, Rahman Z. Influence of the RF excitation of the catalyst system on the morphology of multiwalled carbon nanotubes. *J Phys Chem C* 2007;111:17970–17975.
49. Xu Y, Li ZR, Dervishi E, Saini V, Cui JB, Biris AR, Lupu D, Biris AS. Surface area and thermal stability effect of the MgO supported catalysts for the synthesis of carbon nanotubes. *J Mater Chem* 2008;18:5738–5745.
50. Sun Q, Wang YA, Li LS, Wang DY, Zhu T, Xu J, Yang CH, Li YF. Bright, multi-coloured light-emitting diodes based on quantum dots. *Nat Photonics* 2007;1:717–722.
51. Xu Y, Karmakar A, Wang DY, Mahmood MW, Watanabe F, Zhang YB, Fejleh A, Fejleh P, Li ZR, Kannarpady G, Ali S, Biris AR, Biris AS. Multifunctional Fe₃O₄ cored magnetic-quantum dot fluorescent nanocomposites for RF nanohyperthermia of cancer cells. *J Phys Chem C* 2010;114:5020–5026.
52. Blackman B, Battaglia D, Peng XG. Bright and water-soluble near IR-emitting CdSe/CdTe/ZnSe type-II/type-I nanocrystals, tuning the efficiency and stability by growth. *Chem Mater* 2008;20:4847–4853.
53. Pan BF, Cui DX, He R, Gao F, Zhang YF. Covalent attachment of quantum dot on carbon nanotubes. *Chem Phys Lett* 2006;417:419–424.
54. Karstens T, Kobs K. Rhodamine-B and rhodamine-101 as reference substances for fluorescence quantum yield measurements. *J Phys Chem* 1980;84:1871–1872.
55. Biju V, Itoh T, Baba Y, Ishikawa M. Quenching of photoluminescence in conjugates of quantum dots and single-walled carbon nanotube. *J Phys Chem B* 2006;110:26068–26074.
56. Nikoobakht B, Burda C, Braun M, Hun M, El-Sayed MA. The quenching of CdSe quantum dots photoluminescence by gold nanoparticles in solution. *Photochem Photobiol* 2002;75:591–597.
57. Benediktyova Z, Nedbal L. Imaging of multi-color fluorescence emission from leaf tissues. *Photosynth Res* 2009;102:169–175.
58. Carbajal D, Morano KA, Morano LD. Indirect immunofluorescence microscopy for direct detection of *Xylella fastidiosa* in xylem sap. *Curr Microbiol* 2004;49:372–375.
59. French CJ, Elder M. Virus particles in guttate and xylem of infected cucumber (*Cucumis sativus* L.). *Ann Appl Biol* 1999;134:81–87.
60. Gould N, Minchin PEH, Thorpe MR. Direct measurements of sieve element hydrostatic pressure reveal strong regulation after pathway blockage. *Funct Plant Biol* 2004;31:987–993.
61. Minchin PEH, Thorpe MR. Using the short-lived isotope (¹¹C) in mechanistic studies of photosynthate transport. *Funct Plant Biol* 2003;30:831–841.
62. Doonan JH, Sablowski R. Walls around tumours—why plants do not develop cancer. *Nat Rev Cancer* 2010;10:794–802.
63. Krivacic RT, Ladanyi A, Curry DN, Hsieh HB, Kuhn P, Bergsrud DE, Kepros JF, Barbera T, Ho MY, Chen LB, Lerner RA, Bruce RH. A rare-cell detector for cancer. *Proc Natl Acad Sci USA*. 2004;101:10501–10504.